Optical excitation of surface plasma waves in layered media

G. J. Kovacs and G. D. Scott
Department of Physics, University of Toronto, Toronto, Canada M5S 1A7
(Received 3 January 1977)

The method of frustrated total reflection is used to optically excite electromagnetic surface plasma waves (SPW) in two different layered structures. The first system studied has two films (MgF_2-Ag) between glass and air, and the second has three films (Ag-MgF_2-Ag) between glass and air. Surface roughness of the evaporated MgF_2 films is found to increase with film thickness and this roughness has a pronounced effect on the SPW resonances. A cermet is imagined to form at the MgF_2-Ag interface, and its effective optical constants can be evaluated using the Maxwell Garnett theory. If this cermet is treated as a separate layer in the structure, then good agreement is found with the experimentally observed resonances. A calculation of the Poynting vector field, current distributions, and surface charge densities, resulting from an incident monochromatic plane wave, shows the different modes of oscillation corresponding to each resonance.

I. INTRODUCTION

Optical excitation of surface plasma waves (SPW) by the method of frustrated total reflection was first demonstrated by Otto.[1] He used a very thick film of Ag onto which he pressed the base of a totally reflecting quartz prism. Kretschmann[2] showed that SPW could be excited in a thin Ag film evaporated onto the base of a totally reflecting quartz half-cylinder. Abelès[3] subsequently demonstrated the decoupled optical excitation of SPW at the two surfaces of a thin Au film. In such experiments the total internal reflection of monochromatic light polarized parallel to the plane of incidence is measured as a function of angle. When a SPW is excited, a sharp dip is observed in the reflectance. Under this condition the energy of the incident beam is fed into the surface wave and the total reflection is frustrated.

We extend the study of SPW by first demonstrating the effect of a surface roughness layer on the reflectance resonance. The surface of an evaporated MgF_2 film is quite porous,[4,5] and when Ag is evaporated on top of MgF_2, it will tend to fill the small holes and pits on the MgF_2 surface. Hence, the composite layer can be imagined as a very thin cermet[6] at the MgF_2-Ag interface. The effective optical constants of this cermet layer are then evaluated by the Maxwell Garnett[7] theory, which applies to small metal particles embedded in a dielectric. The induced roughness on the top surface of the Ag film is then treated as a roughness layer and its effective optical constants can likewise be evaluated by the Maxwell Garnett theory. In the latter case, the dielectric MgF_2 is replaced by air. The experimentally measured resonances or dips, are generally shifted to larger angle and may be damped as compared with what is predicted by theory based on the measured thicknesses and known optical properties of MgF_2 and Ag. The insertion of the cermet and roughness layers gives a good account of the experimentally observed shifting and damping of the resonances.

We then make a calculation of the electric and magnetic field components throughout the entire film system. An incident monochromatic plane wave is assumed and Maxwell's equations with appropriate boundary conditions yield the $\vec{E}$ and $\vec{H}$ fields. The Poynting vector field $\vec{S}$ gives the time-averaged energy flux of the electromagnetic field. A calculation of $\vec{S}$ for the conditions at a resonance minimum shows at which surface(s) the SPW is excited. By knowing in which region the energy flux is concentrated we can understand the effects which surface roughness will produce on the resonances. If an excitation is localized very strongly to a particular surface, and if this surface is a rough one, we might expect discrepancies from a first calculation which assumes a perfect planar interface.

Although the Poynting vector can give considerable information about the nature of an excitation in a film system, it does not give a complete description. Surface plasma waves which are coupled between two surfaces may show quite similar Poynting vector profiles (see Figs. 15 and 16), but the nature of the oscillations can be quite different (see Figs. 17 and 18). Therefore, we also calculated the current distributions and surface charge densities associated with the electromagnetic field. The $\vec{E}$ field of the incident radiation induces microscopic currents in the film system. Moreover, light polarized with a component of $\vec{E}$ perpendicular to the film surface will cause a surface charge density to be created at an interface between two different media. These current distributions and surface charge densities give a more complete description of the SPW oscillations.

II. EXPERIMENTAL RESULTS

In our experiments we employed two arrangements of the films as shown in Fig. 1. All samples were formed by successive thermal evaporation onto room-temperature substrates in conventional high vacuum. Prism substrates were ultrasonically cleaned with both alconox solution and distilled water, then degreased with alcohol vapor, then finally baked at 150 °C for three hours in high vacuum. By a vacuum seal movement we were able to form a duplicate of each evaporated film so that their thicknesses could be measured separately. All film thicknesses were measured by the FECO (fringes of equal chromatic order) method using an instrument described previously by Scott.[8]

When investigating the optical excitation of SPW, we measured, as a function of angle, the reflectivity of p-polarized light, since there are no surface modes of s character.[9] The vacuum wavelength of the incident light was chosen as 495 nm so that the observed resonances would lie in a conveniently measured angular region. A typical measured reflectance for a two-film system is shown in Fig. 2. The accompanying theoretical curve is calculated with the Fresnel equations, using the index of refraction of the glass, and that of MgF_2 (taken as 1.38),[10] the optical constants of Ag as given most recently by Johnson and Christy,[11] and the measured film thicknesses. The first dip near 33°, occurs due to the excitation of a SPW at the Ag-air interface; the second dip due to the excitation of a SPW at the Ag-MgF_2 interface.[3] The first peak corresponds to the onset of total internal reflection and occurs at the critical angle of approximately 31°. Both experimentally observed resonances are shifted to larger angles than given by the calculated curve. This shift in the resonances we attribute to the roughness on the top surface of the evaporated MgF_2 film and the corresponding induced roughness on the top surface of the Ag film.

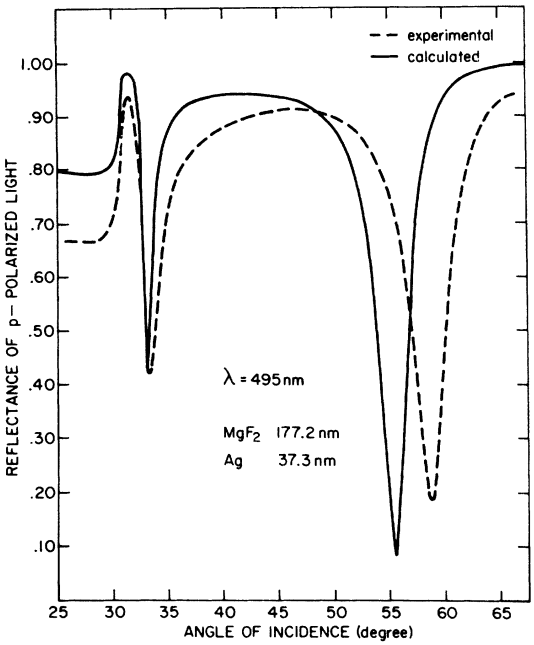

FIG. 2. Experimental and calculated reflectance as a function of angle for a two-film system. The measured film thicknesses and the wavelength of light used are indicated.

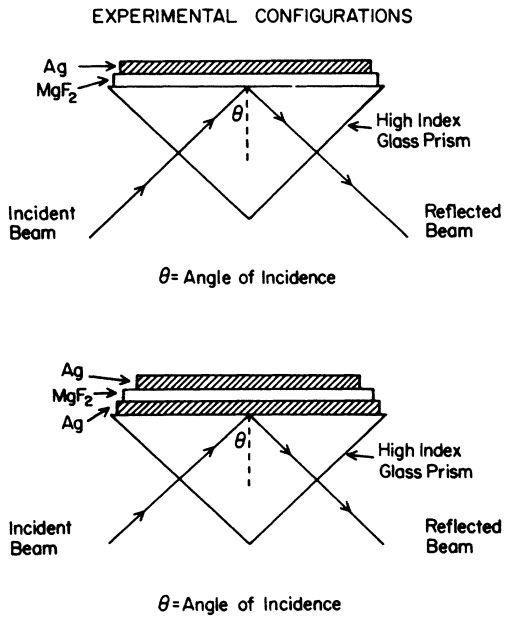

FIG. 1. Two configurations of evaporated films which were studied.

We found that the surface roughness of the MgF_2 films increased with their thickness. This is illustrated by the transmission electron micrographs of the MgF_2 surface shown in Fig. 3. The micrographs were made from platinum shadow-cast carbon replicas of the surface of the MgF_2 films, starting first with an uncoated substrate and then increasingly thicker films up to a thickness of about 740 nm. The roughness is on a very fine scale, much smaller than the wavelength of light used, and we therefore expect the scattering of light to be quite small, with the total scattering less than 0.1%.[12] Therefore, we neglect scattering and introduce a cermet layer between the Ag and MgF_2 and a roughness layer between the Ag and air. The effective optical constants of these two pseudolayers are then evaluated by the Maxwell Garnett theory. According to the Maxwell Garnett calculation, ϵ_c, the effective dielectric constant

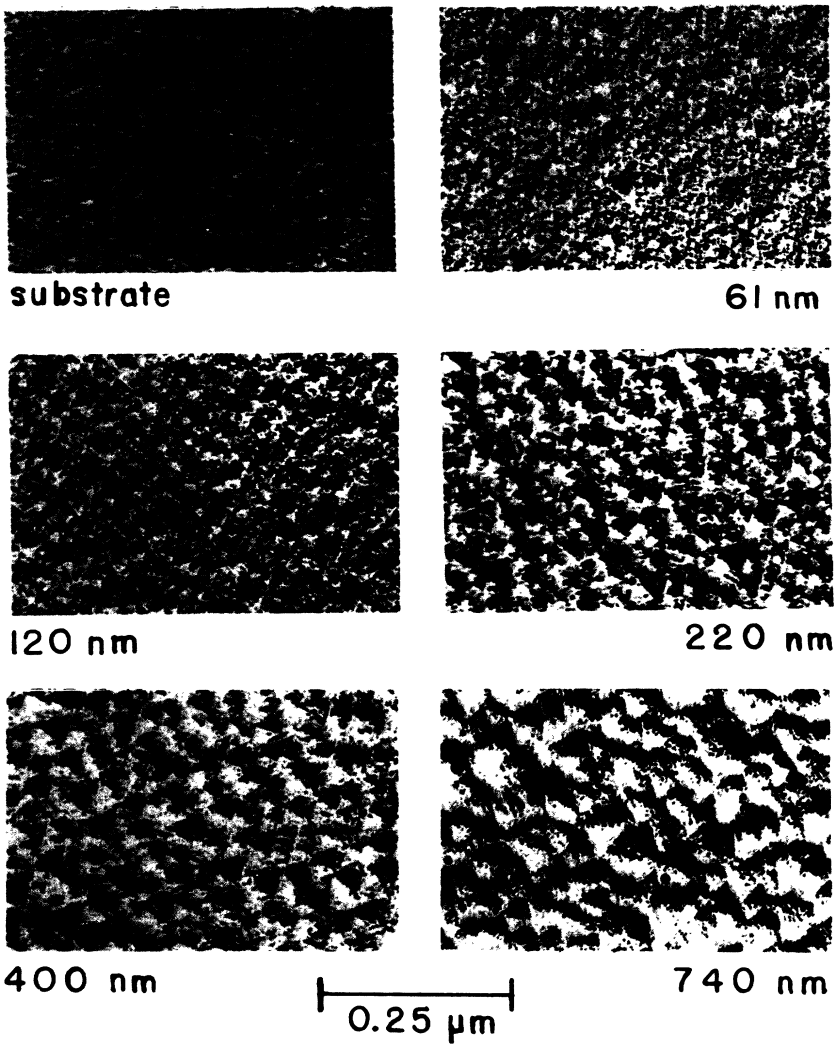

FIG. 3. Electron micrographs of platinum shadow-cast carbon replicas of the surface of a series of MgF_2 films. The thickness of the films is indicated.

of the cermet, is given by

$$\epsilon_c = \epsilon_D[\epsilon_M(1+2q)+2\epsilon_D(1-q)]/[\epsilon_M(1-q)+\epsilon_D(2+q)], \tag{1}$$

where ϵ_D is the dielectric constant (real) of the nonconducting material of the cermet, ϵ_M is the complex dielectric constant of the metallic constituent, and q is the volume fraction of the metallic constituent. In all cases the thickness of the roughness layer was taken as half that of the cermet layer. This is reasonable since the Ag film has a smoothing effect on the MgF_2 surface.

If we take the same experimental results as in Fig. 2 now and plot with that the reflectivity of a four-film system, we get the result shown in Fig. 4. The MgF_2 and Ag film thicknesses have been adjusted appropriately to allow for formation of the cermet and roughness layers. The filling factor q was taken as 0.4 for the cermet and 0.6 for the roughness. The agreement with experiment is much better. It should be noted that a Ag_2S tarnish of 10 Å would account for the observed shift in the first resonance. However, we have made a detailed study of the growth of Ag_2S tarnish in our laboratory by observing the shift in the SPW resonance for a single Ag film as a function of time. From the known optical constants of Ag_2S,[13] we determined that the tarnish layer grows at an average rate of about 5 Å per week for several weeks. Since all samples were measured within a few hours of removal from high vacuum, Ag_2S cannot be contributing significantly to the observed resonance shift. The effect of absorbed water vapor on the exposed Ag surface is also thought to be quite small.[14]

The increase of surface roughness with increasing MgF_2 thickness is illustrated in Fig. 5 where

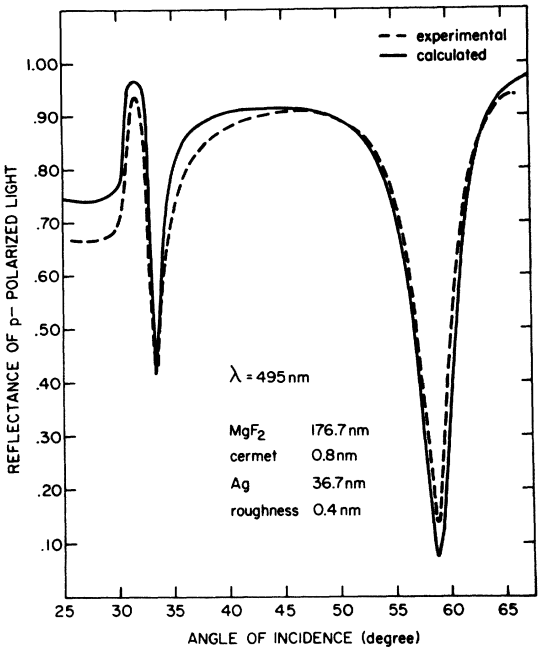

FIG. 4. Experimental reflectance from Fig. 2 and calculated reflectance now using cermet and roughness layers ($q = 0.4$ for cermet and $q = 0.6$ for roughness).

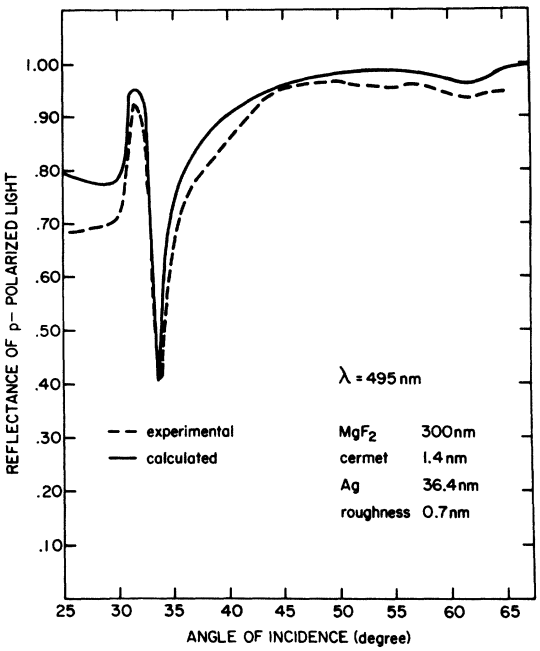

FIG. 6. Experimental reflectance from Fig. 5 and calculated reflectance now using cermet and roughness layers ($q = 0.4$ for cermet and $q = 0.6$ for roughness).

the calculated curve shows two SPW resonances again, but the experimental curve shows only one. The MgF_2 film is about 70% thicker than in the previous case (Fig. 2), but the Ag film thickness is exactly the same since the Ag films of both samples were formed during the same evaporation. If we increase our cermet and roughness thicknesses by approximately 70% and use the same q values as previously, i.e., 0.4 and 0.6 for cermet and roughness, respectively, we get the improved fit shown in Fig. 6. Notice that the SPW resonance at the Ag-MgF_2 interface has been completely wiped out by the cermet layer.

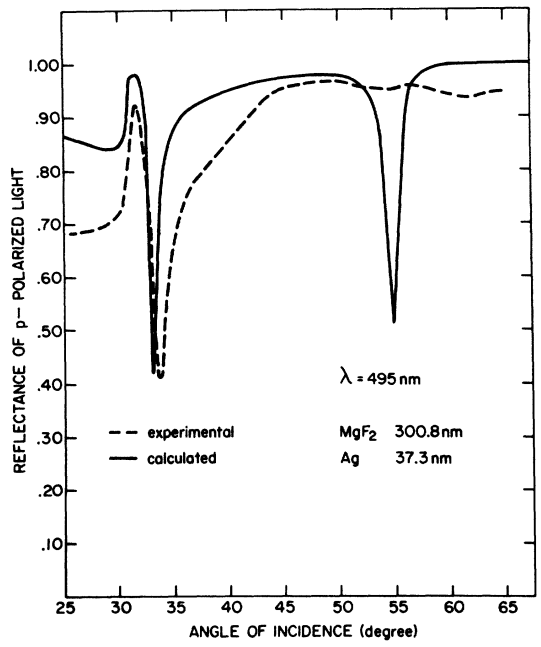

FIG. 5. Experimental and calculated reflectance for a second two-film system.

A triple film system Ag-MgF_2-Ag can be treated in a similar way: the theoretical to experimental results are compared in Figs. 7 and 8. The shift to larger angles of all three resonances and the damping of the final resonance are accounted for by the cermet and roughness layers. The q values used in Fig. 8 are again 0.4 and 0.6, respectively. If we again consider a Ag-MgF_2-Ag combination only now with a considerably thicker MgF_2 film, we get the results shown in Figs. 9 and 10. The shift to larger angles of the first four resonances can again be accounted for. The values of q used in Fig. 10 were taken as 0.42 and 0.1, respectively.

III. THEORETICAL CALCULATIONS

A. Two films

We stated that the first dip in Fig. 2 is due to the excitation of a SPW at the Ag-air interface and that the second is due to a SPW at the Ag-MgF_2 in-

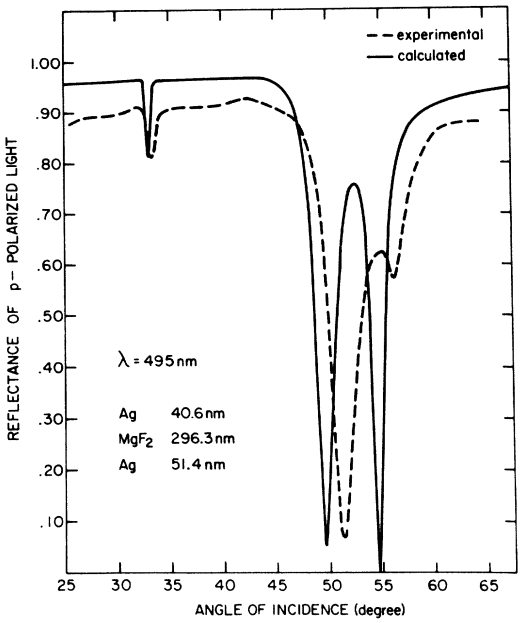

FIG. 7. Experimental and calculated reflectance for a three-film system.

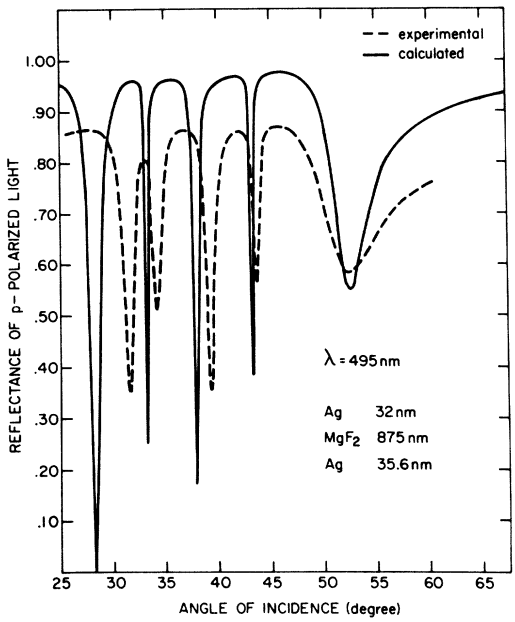

FIG. 9. Experimental and calculated reflectance for a second three-film system.

terface. In order to illustrate the nature of these resonances, we consider an obliquely incident monochromatic plane wave polarized in the plane of incidence. The incident wave propagates through the glass making an angle θ with the normal (see Fig. 1). Using the Maxwell equations,[15] we can calculate the incident, reflected and transmitted, electric and magnetic fields in each of the media. The Poynting vector field $\vec{S}$ can then be computed from the $\vec{E}$ and $\vec{H}$ fields for any angle of incidence.

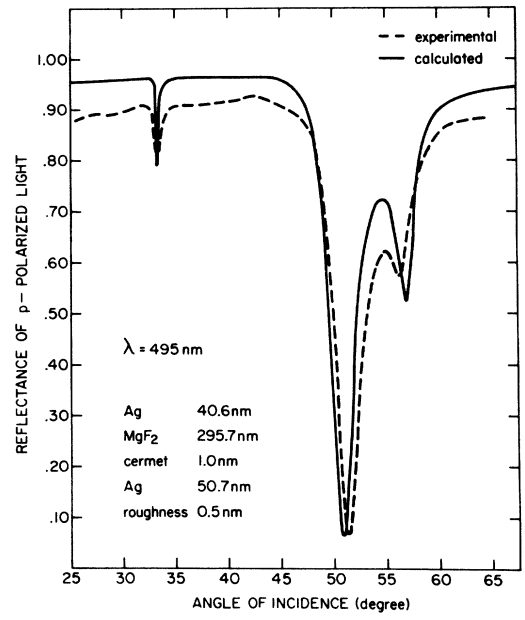

FIG. 8. Experimental reflectance from Fig. 7, and calculated reflectance now using cermet and roughness layers ($q = 0.4$ for cermet and $q = 0.6$ for roughness).

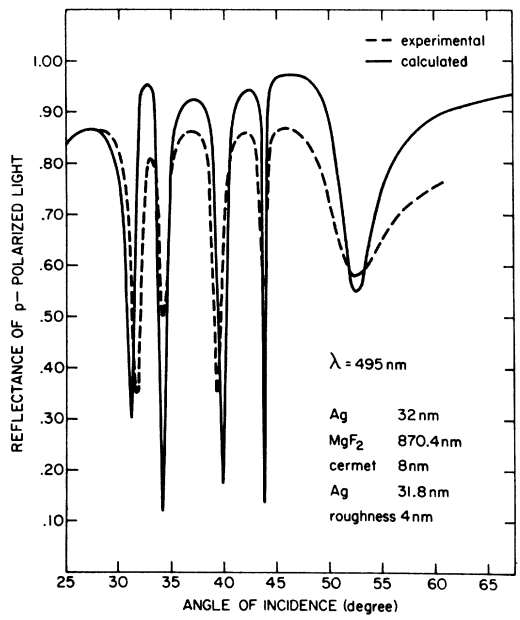

FIG. 10. Experimental reflectance from Fig. 9, and calculated reflectance now using cermet and roughness layers ($q = 0.42$ for cermet and $q = 0.1$ for roughness).

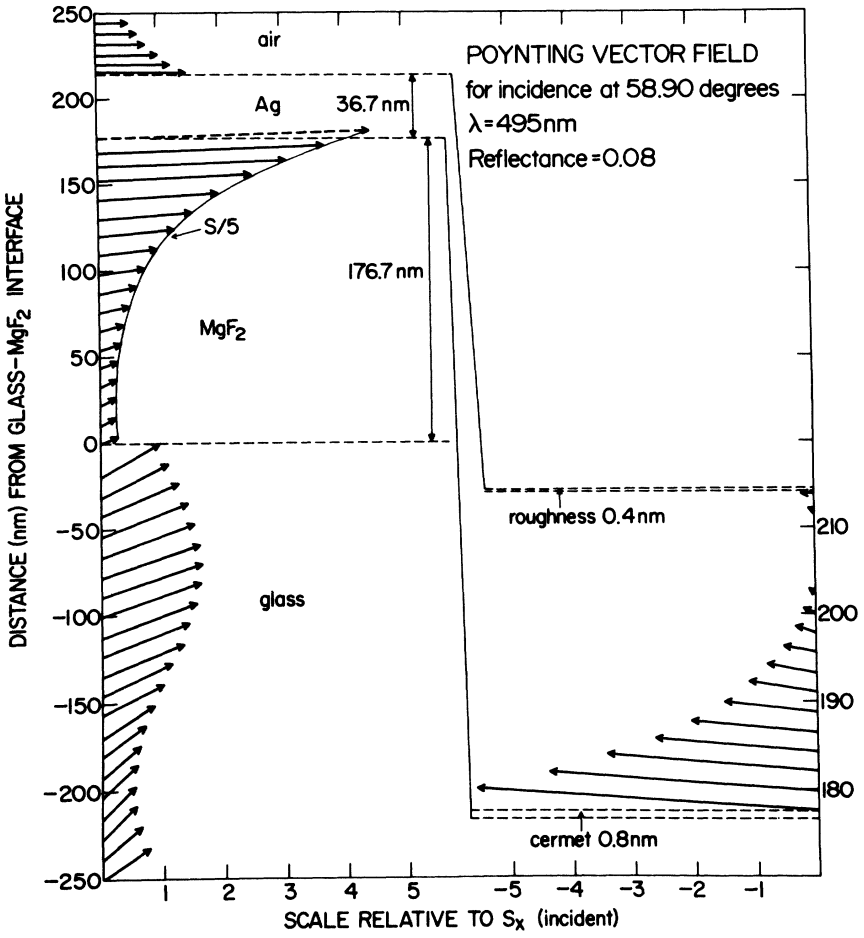

FIG. 11. Poynting vector field for second minimum of theoretical curve of Fig. 4.

$$\vec{S} = (c/8\pi)\,\mathrm{Re}(\vec{E} \times \vec{H}^*) . \qquad (2)$$

If at a given angle the energy flux of the electromagnetic field is concentrated at a surface, we interpret this to mean that a SPW is excited at that surface.

The Poynting vector field for the theoretical curve of Fig. 4 at an angle of incidence of 58.90°, i.e., at the position of the second minimum, is illustrated in Fig. 11. Since we consider an infinite plane wave, the only variation in the Poynting vector field is in the z direction, i.e., the direction perpendicular to the plane of the films. The Poynting field in the incident medium always displays an oscillatory behavior due to the overlap of incident and reflected fields. The high concentration of energy flux at the MgF_2-Ag interface corresponds to a SPW excitation there. Note the negative direction of the energy flow in the metal film shown on the lower right in an expanded view. This is a direct consequence of the fact that the metal has a negative real part of the dielectric constant. Note also the evanescent field in the final medium, which is air. The scale of the Poynting field is relative to that of the horizontal or x component of the incident Poynting vector. Each vector represents the field strength at the position of its base, and if sometimes a vector is of such a length as to run into an adjacent medium, it is denoted there by a dashed line.

The Poynting vector field for the first dip of the theoretical curve of Fig. 5 is illustrated in Fig. 12. The large energy flux at the Ag-air interface indicates a SPW there. The Poynting vector in the dielectric is roughly ten times the magnitude and in the opposite direction to that in the metal. Hence, the net energy flux of the SPW is in the same direction as that of the incident beam as we would expect.

We can also use the expressions for the electric field $\vec{E}$ given by a complete solution of the Maxwell equations to calculate the current density $\vec{J}$ in each medium. The induced polarization current is given by

$$\vec{J} = [i\omega(1-\epsilon)/4\pi]\vec{E} . \qquad (3)$$

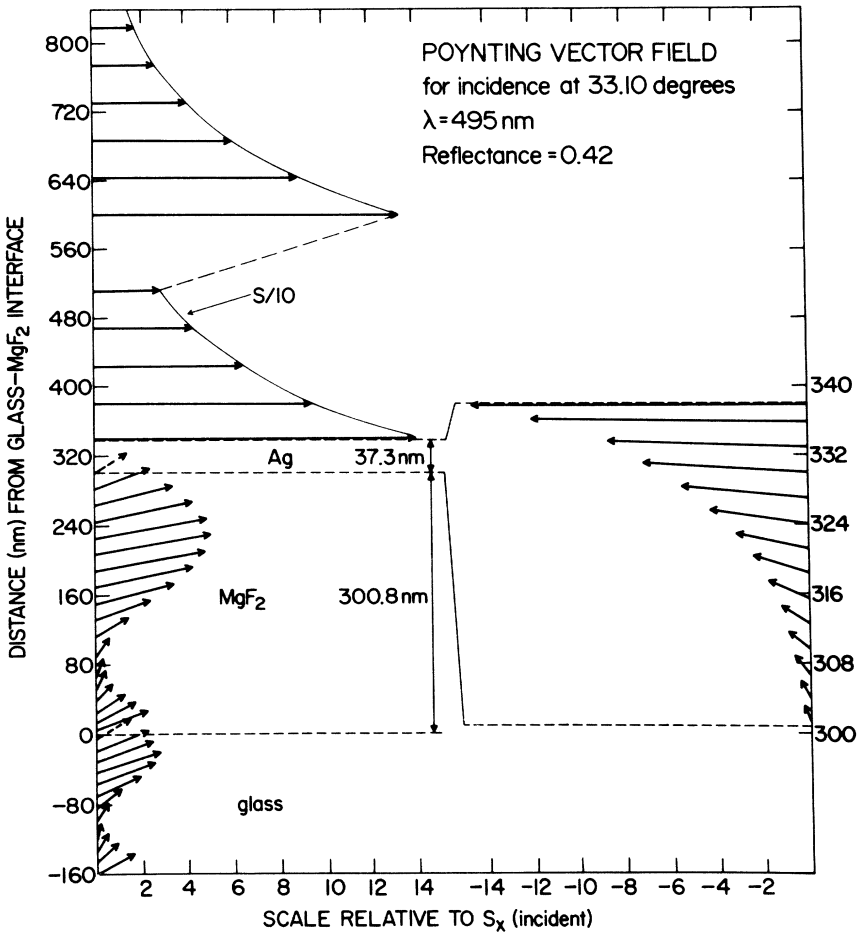

FIG. 12. Poynting vector field for first minimum of theoretical curve of Fig. 5.

This polarization current is zero in the air ($\epsilon = 1$) and it is exactly 90° out of phase with the electric field $\vec{E}$ in other dielectric media ($\epsilon > 1$). For Ag, which has a small imaginary part of the dielectric constant ($\epsilon = -9.564 + 0.309i$ at $\lambda = 495$ nm),[11] there is a small fraction of the current which is in phase with $\vec{E}$, but the major portion is still out of phase with $\vec{E}$. In general the currents are larger in the Ag than the MgF_2 because the metal has a large negative real part of the dielectric constant and the MgF_2 has a relatively small positive dielectric constant. The induced surface charge density $\hat{\rho}$ at the interface between the j and $j+1$ medium is given by the expression

$$\hat{\rho} = (E_z^{(j+1)} - E_z^{(j)})/4\pi \, . \tag{4}$$

The discontinuity of the component of the electric field normal to the surface gives rise to the surface charge density.

The current distributions and surface charge densities calculated for the two resonance angles of the theoretical curve of Fig. 2 are shown in Fig. 13. They are illustrated for the Ag film, and the upper portion of the MgF_2 dielectric film. The arrows everywhere point in the direction of the current $\vec{J}$ and their thickness is proportional to the magnitude of the current. The thickness of the (+) and (−) signs is also proportional to the magnitude of the surface charge density. For the first resonance, the currents and charge densities are peaked at the Ag-air interface; for the second, they are peaked at the Ag-MgF_2 interface.

B. Three films

We can now analyze by similar techniques the resonances of the three-film systems. The first small resonance of Fig. 7 is due to a SPW at the final Ag-air interface and the shift to larger angles is accounted for by the roughness layer as shown in Fig. 8. From the theoretical curve of Fig. 7 we calculate the Poynting vector field for incidence at 54.70°, i.e., at the position of the third minimum. It is shown in Fig. 14 that this resonance

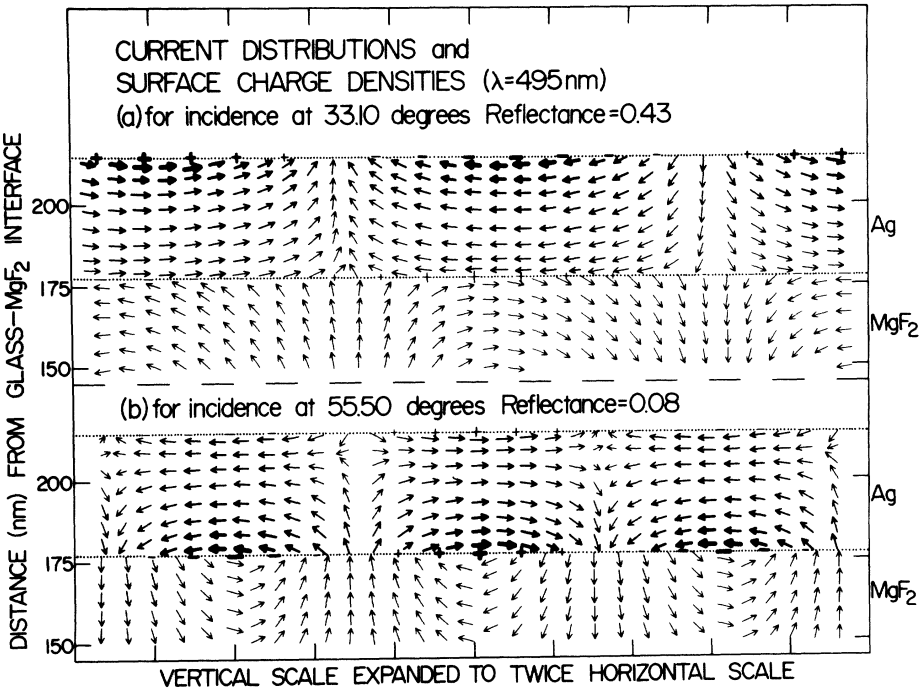

FIG. 13. Current distributions and surface charge densities for both minimums of theoretical curve of Fig. 2.

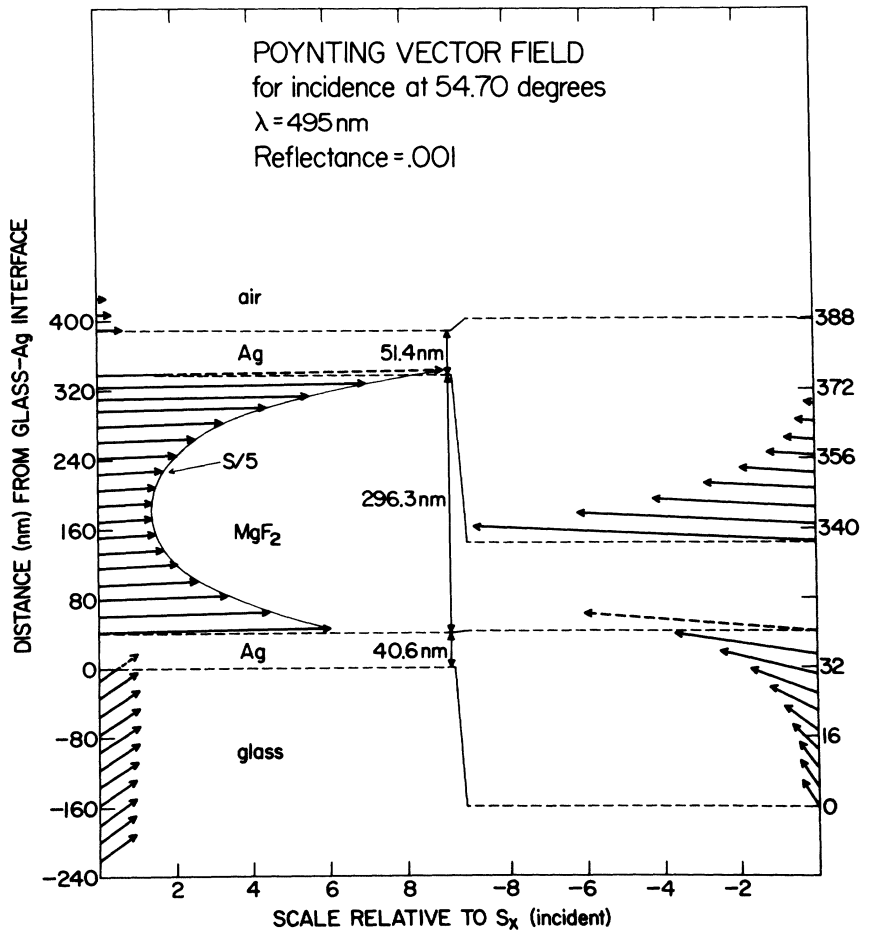

FIG. 14. Poynting vector field for third minimum of theoretical curve of Fig. 7.

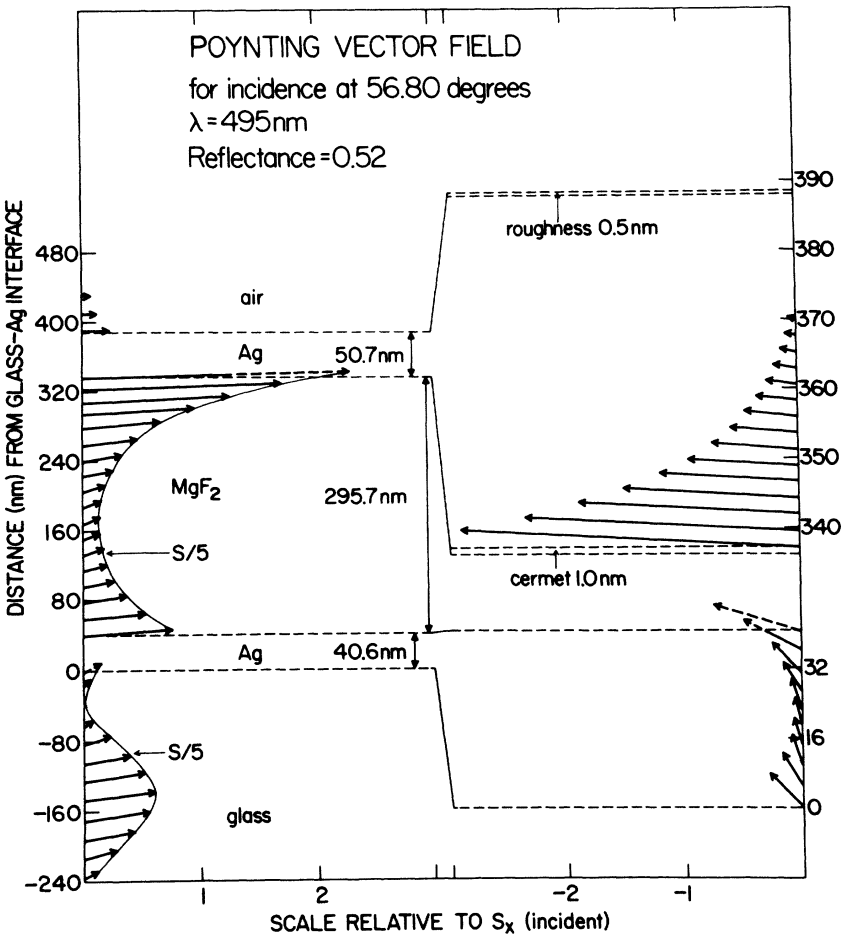

FIG. 15. Poynting vector field for third minimum of theoretical curve of Fig. 8.

corresponds to a coupled excitation at the two surfaces of the MgF_2 with the energy flux greater at the second MgF_2-Ag interface. Since the energy is concentrated at the top surface of the MgF_2 which we know to be rough we would expect this resonance to be strongly affected by the addition of a cermet layer. This is indeed the case as we saw in Fig. 8 where the curve calculated using cermet and roughness layers shows the final resonance to be weakened considerably. The Poynting vector field calculated with cermet and roughness layers for the final resonance of the theoretical curve of Fig. 8 is shown in Fig. 15. The excitation has the same general profile, but has greatly reduced intensity relative to that of the incident flux. (Compare the horizontal scale of Figs. 14 and 15.) The Poynting vector field for the second resonance of Fig. 8 is shown in Fig. 16. The main energy flux is concentrated at the lower MgF_2 surface which is smooth; hence, this resonance is not as affected as the third resonance which has higher energy flux at the top MgF_2 surface. The Poynting vector field for the second resonance without cermet is very similar to Fig. 16, the only change being slightly larger energy flux at the top MgF_2 surface. The current distributions and surface charge densities for the second and third resonances of the theoretical curve of Fig. 7 are shown in Figs. 17 and 18, respectively. The SPW of Fig. 17 is a symmetric type of oscillation coupled to the two surfaces of the MgF_2. Regions of similar surface charge density are directly across from each other. The SPW in Fig. 18 is a coupled oscillation of an antisymmetric type with regions of opposite charge density directly across from each other.

The final experiment which we wish to consider again involves an Ag-MgF_2-Ag system, but the MgF_2 thickness is now considerably larger than in the previous case. The experimental results and calculated curves are shown in Figs. 9 and 10. With the increased thickness of the dielectric, two new types of resonances occur. The first dip of the theoretical curve of Fig. 9 corresponds to a

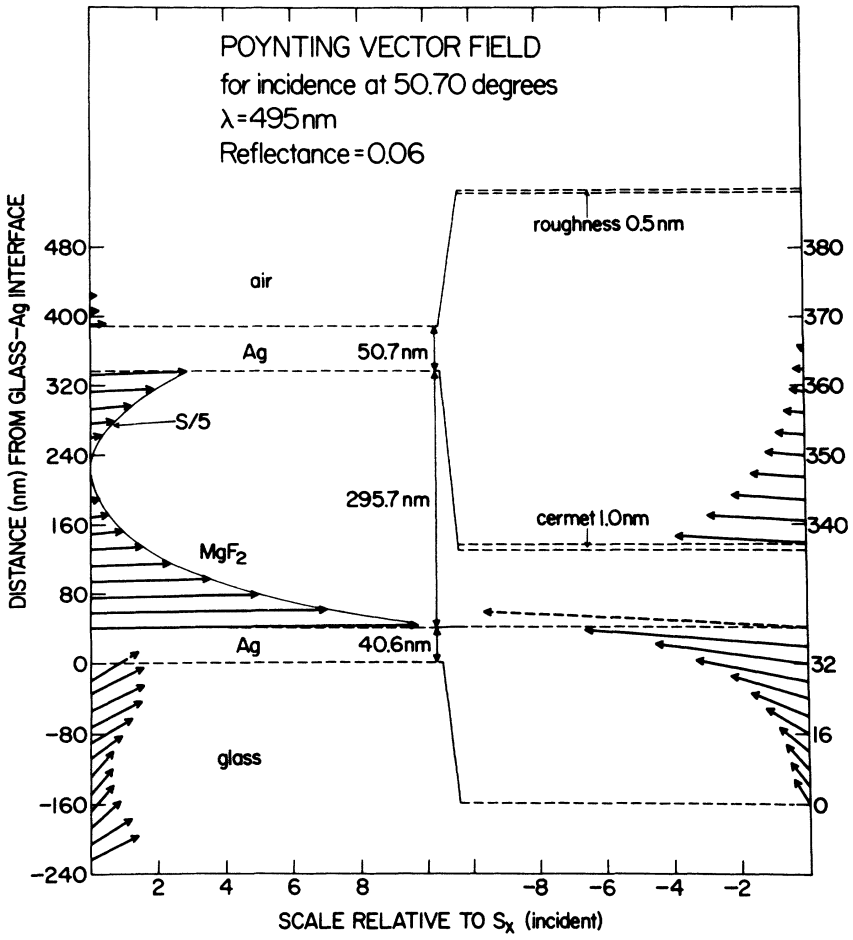

FIG. 16. Poynting vector field for second minimum of theoretical curve of Fig. 8.

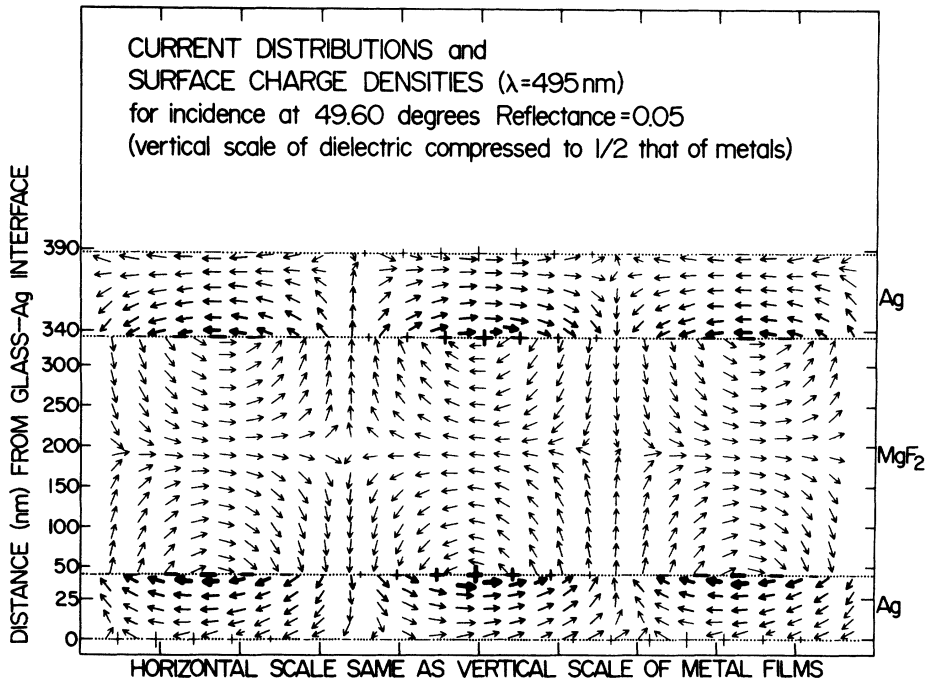

FIG. 17. Current distributions and surface charge densities for second minimum of theoretical curve of Fig. 7.

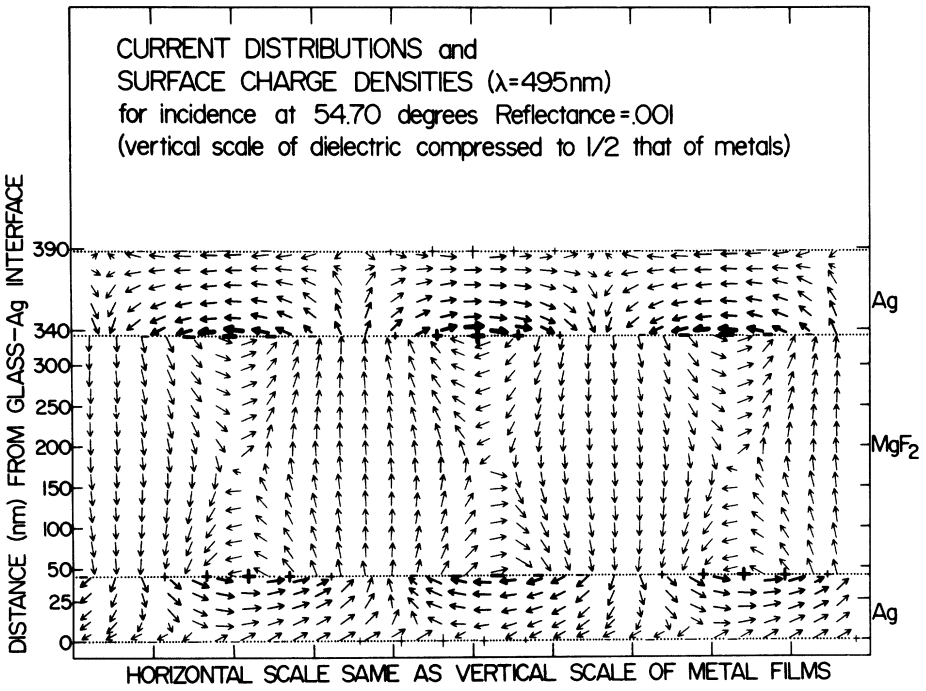

FIG. 18. Current distributions and surface charge densities for third minimum of theoretical curve of Fig. 7.

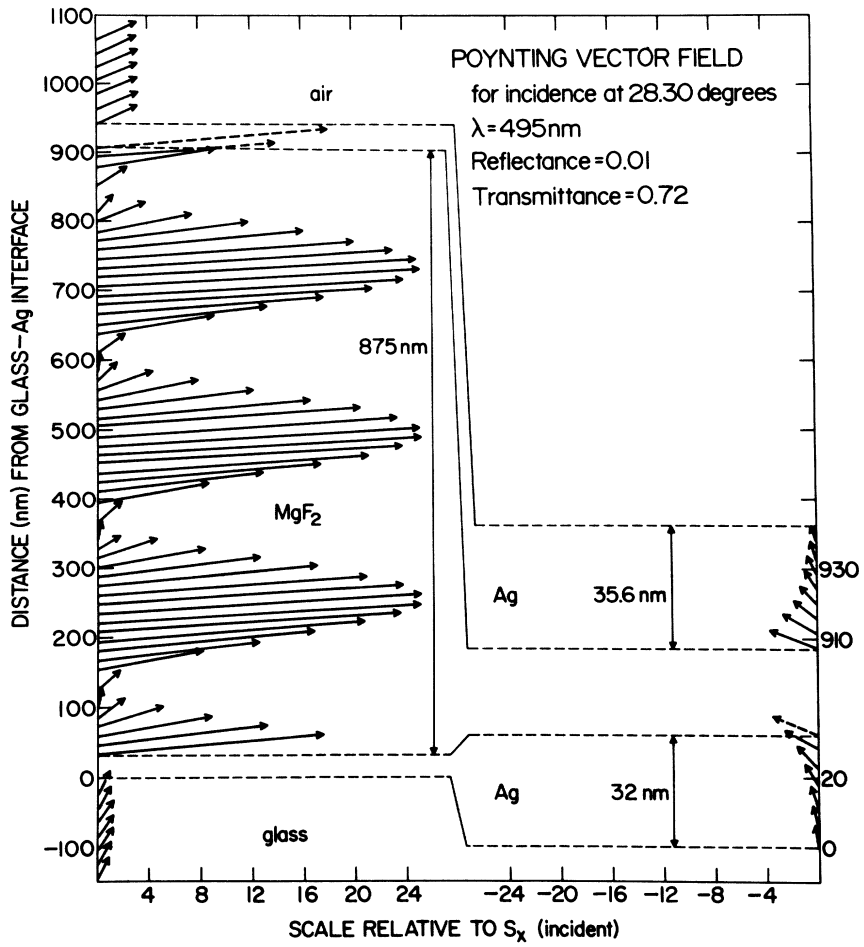

FIG. 19. Poynting vector field for first minimum of theoretical curve of Fig. 9.

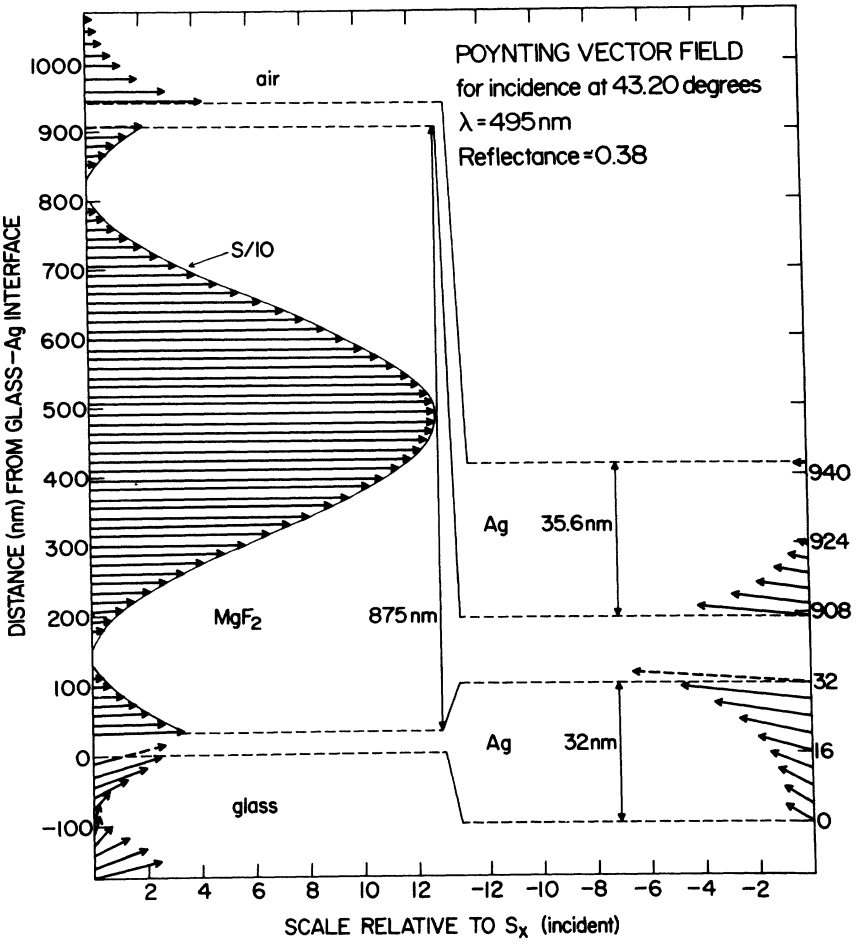

FIG. 20. Poynting vector field for fourth minimum of theoretical curve of Fig. 9.

resonance transmission at an angle less than the critical angle. The Poynting vector field for this resonance is shown in Fig. 19. A transmittance of 72% is predicted by theory, but no peak in transmittance was observed experimentally. This is due to the fact that the first dip in the experimentally measured reflectance occurs at an angle greater than the critical angle, and this is accounted for by the calculated curve of Fig. 10 using cermet and roughness layers. If the Poynting vector field for the first dip of the theoretical curve of Fig. 10 is calculated, we get a distribution similar to that of Fig. 19. However, the three peaks of the field in the MgF_2 have greatly reduced intensity and the transmitted field is replaced by a large evanescent field.

The second new type of resonance which occurs is due to guided modes in the dielectric layer. The term guided is used to mean that the energy flux is concentrated within the dielectric layer rather than at its surface. The Poynting vector field for the fourth dip of the theoretical curve of Fig. 9 is shown in Fig. 20. The current distributions and surface charge densities for this first guided mode are shown in Fig. 21. This oscillation is coupled antisymmetrically to the two surfaces of the MgF_2 film in contact with the Ag. The Poynting vector field for the third dip of the theoretical curve of Fig. 9 is shown in Fig. 22. The current distributions and surface charge densities for this second guided mode are shown in Fig. 23. This oscillation is coupled symmetrically to the two surfaces of the dielectric in contact with the metal.

The second dip in Fig. 9 is due to excitation of a SPW at the final Ag-air interface and it is shifted to larger angles by the roughness layer in Fig. 10. The fifth broad dip is due to excitation of a SPW at the first Ag-MgF_2 interface with the fields decaying completely by the upper region of the MgF_2. This latter excitation is localized to the lower MgF_2 interface, which we expect to be smooth. Since it does not extend to the upper surface of the MgF_2, it should be unaffected by surface roughness at the top. This is indeed the case as this resonance

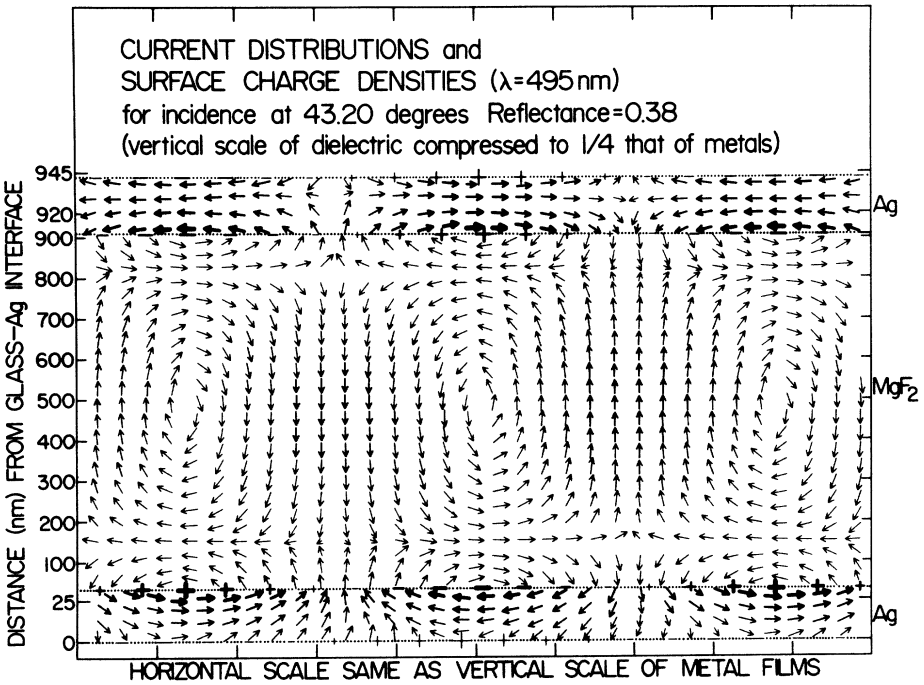

FIG. 21. Current distributions and surface charge densities for fourth minimum of theoretical curve of Fig. 9.

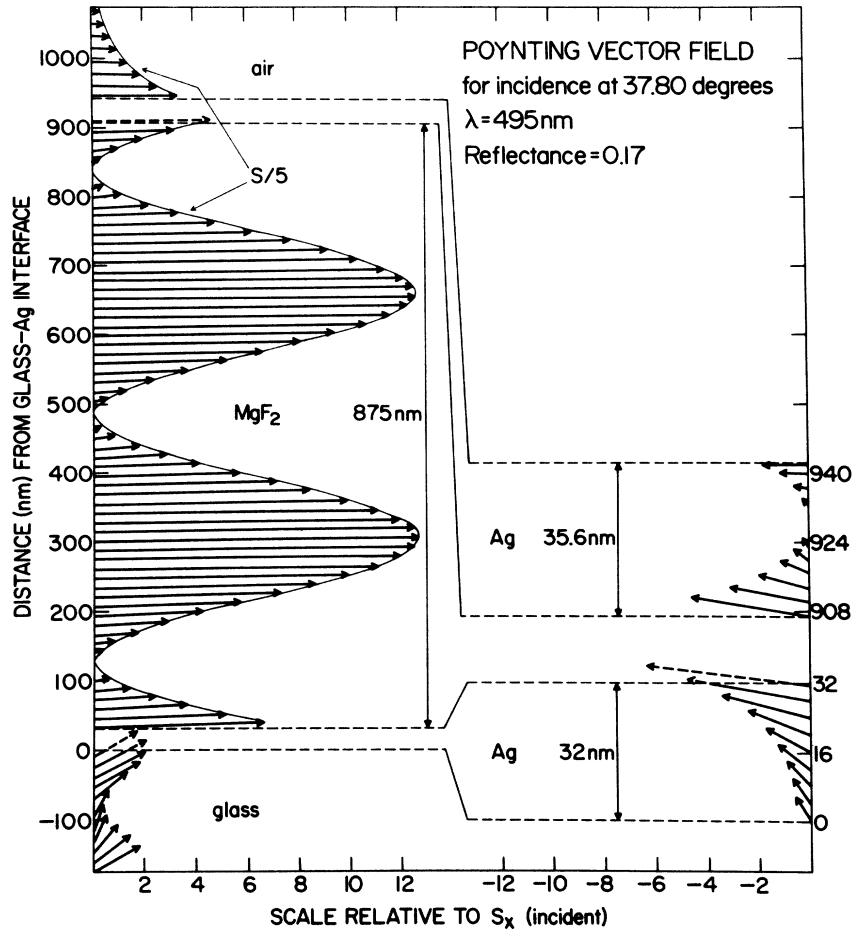

FIG. 22. Poynting vector field for third minimum of theoretical curve of Fig. 9.

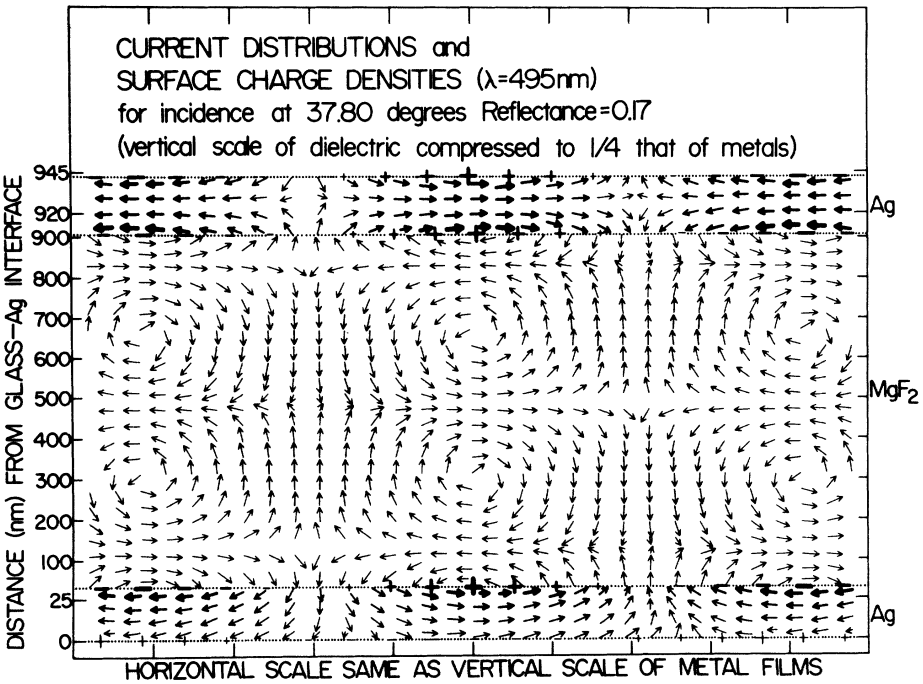

FIG. 23. Current distributions and surface charge densities for third minimum of theoretical curve of Fig. 9.

maintains the same shape and position in Fig. 10 that it has in Fig. 9.

The theoretical curve of Fig. 9 shows another resonance in the reflection at 10.90°. The reflectance at that angle dips to 2%, and the transmittance peaks to 65%. The Poynting vector field is similar to that of Fig. 19, only with four peaks in the energy flux across the MgF_2 layer instead of three. The first guided mode at 43.20° has one peak in the energy flux (Fig. 20); the second guided mode at 37.80° has two peaks (Fig. 22); the resonance transmission at 28.30° has three peaks (Fig. 19), and the resonance transmission at 10.90° has four peaks (not shown). It is found that with increasing dielectric thickness a resonance transmission moves to larger angles until it passes the critical angle and becomes the next guided mode. As the dielectric thickness increases, the resonance transmission of Fig. 19 will become the third guided mode and the resonance transmission at 10.90° will move up to become the fourth guided mode.

IV. CONCLUSIONS

The method of frustrated total reflection has been used to excite SPW in two different film systems. This technique is very sensitive to the surface roughness of evaporated films. The observed resonances are shifted and may be damped relative to those predicted by theory, assuming a perfect planar interface separating the metal from the dielectric. We have accounted for these discrepancies in a systematic way by introducing the cermet and roughness layers. A calculation of the Poynting vector field shows the localization of the excitation corresponding to each resonance. Knowing the region where the energy flux is concentrated allows us to understand the effect which surface roughness will have on the experimentally observed resonances in reflectance. The current distributions and surface charge densities induced by the electromagnetic field demonstrate SPW oscillations of a definite symmetry corresponding to resonances in the three-film system. In three-film systems, resonance transmissions and guided modes become possible with thick dielectric films. Moreover, resonance transmissions move to larger angles with increasing dielectric thickness until they pass the critical angle, whereupon they graduate into guided modes.

ACKNOWLEDGMENTS

We wish to thank T. Sato for his generous technical assistance in general, and for preparation of the evaporated films and for the electron microscopy in particular. We would also like to acknowledge the financial support of this study by the National Research Council of Canada.

[1]A. Otto, Z. Phys. 216, 398 (1968).
[2]E. Kretschmann, Z. Phys. 241, 313 (1971).
[3]F. Abelès and T. Lopez-Rios, Opt. Commun. 11, 89 (1974).
[4]K. Kinosita and M. Nishibori, J. Vac. Sci. Technol. 6, 730 (1969).
[5]H. K. Pulker and E. Jung, Thin Solid Films 9, 57 (1971).
[6]P. H. Lissberger and R. G. Nelson, Thin Solid Films 21, 159 (1974).
[7]J. C. Maxwell Garnett, Philos. Trans. R. Soc. Lond. A203, 385 (1904); 205, 237 (1906).
[8]G. D. Scott, *Vacuum Symposium Transactions 1956*, (Pergamon, New York, 1957), p. 24.
[9]K. L. Kliewer and R. Fuchs, Phys. Rev. 153, 498 (1967).
[10]G. Hass and E. Ritter, J. Vac. Sci. Technol. 4, 71 (1967).
[11]P. B. Johnson and R. W. Christy, Phys. Rev. B 6, 4370 (1972).
[12]H. J. Simon and J. K. Guha, Opt. Commun. 18, 391 (1976).
[13]J. M. Bennett, J. L. Stanford, and E. J. Ashley, J. Opt. Soc. Am. 60, 224 (1970).
[14]D. K. Burge, J. M. Bennett, R. L. Peck, and H. E. Bennett, Surf. Sci. 16, 303 (1969).
[15]M. Born and E. Wolf, *Principles of Optics*, 5th ed. (Pergamon, Oxford, 1975), p. 1.

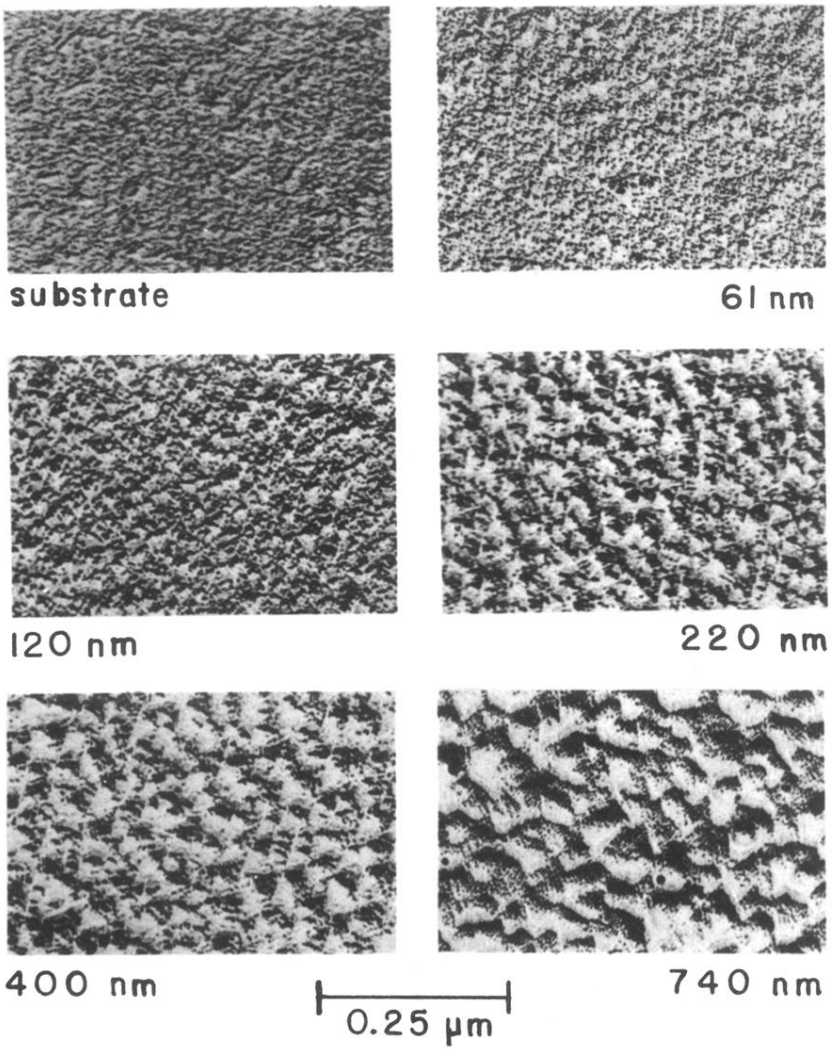

FIG. 3. Electron micrographs of platinum shadow-cast carbon replicas of the surface of a series of MgF_2 films. The thickness of the films is indicated.